Simulations of the photoelectron sheath and dust levitation on the lunar surface

Andrew Poppe[1,2] and Mihály Horányi[1,2]

Received 20 January 2010; revised 26 April 2010; accepted 27 April 2010; published 26 August 2010.

[1] The lunar surface represents a complex plasma environment due to the presence of solar ultraviolet (UV) radiation, the incoming solar wind flux and charged, levitated micron- and sub-micron sized dust particles. Photoemission due to solar UV radiation dominates the charging environment, creating a photoelectron sheath above the lunar surface. To further investigate the dusty plasma environment on the surface of the Moon, a one-dimensional particle-in-cell (PIC) code has been designed specifically for the lunar surface. The code has been validated against analytic solutions for photoelectron sheaths with basic photoelectron energy distributions. Simulations have focused on the role of the emitted photoelectron energy distribution and solar UV variability in determining the sheath profile. Additionally, the charging and levitation of test dust particles in the photoelectron sheath are studied. Limits on the maximum size and height of levitated dust grains are also presented.

Citation: Poppe, A., and M. Horányi (2010), Simulations of the photoelectron sheath and dust levitation on the lunar surface, *J. Geophys. Res.*, *115*, A08106, doi:10.1029/2010JA015286.

1. Introduction

[2] The plasma environment on the Moon is shaped by a combination of processes that vary as it orbits the Earth. On the sunlit side of the Moon while in the solar wind, photoelectric charging due to solar ultraviolet (UV) radiation and the collection of solar wind ions and electrons dominate the creation of the lunar plasma environment. The photoemission current is greater than the current collected from the solar wind and therefore, the sunlit lunar surface is expected to charge positively. A photoelectron sheath will develop near the lunar surface, accelerating electrons towards the moon while retarding ions. Previous work has derived theoretical expressions for the potential and electron density above a photoemitting surface [*Guernsey and Fu*, 1970; *Grard and Tunaley*, 1971; *Walbridge*, 1973] for an assumed Maxwellian energy distribution for the emitted photoelectrons. However, the emitted photoelectron energy distribution for the lunar surface differs from a Maxwellian distribution since it is dependent on the incoming solar flux, the lunar dust work function and the photoelectric yield function [*Feuerbacher et al.*, 1972; *Sternovsky et al.*, 2008]. Additionally, the solar wind flux alters the extent and nature of the photoelectron sheath by providing a flux of ions and electrons to the surface. While previous work has been done on the plasma environment above the lunar surface [*Freeman and Ibrahim*, 1975; *De and Criswell*, 1977; *Criswell and De*, 1977; *Nitter et al.*, 1998; *Borisov and Mall*, 2006; *Farrell et al.*, 2007], a particle-in-cell study, combining the effects of the distinct lunar photoelectron distribution and the inflowing solar wind flux, has not yet been undertaken.

[3] Micron and sub-micron sized dust grains from the lunar regolith are present in and can alter the nature of the lunar photoelectron sheath. These grains charge via photoemission and the collection of electrons and ions, and change the local plasma environment. In-situ experimental evidence suggests that lunar dust grains can be mobilized and transported above the lunar surface [*Criswell*, 1972; *Rennilson and Criswell*, 1974; *Berg et al.*, 1974; *Zook and McCoy*, 1991] and laboratory experiments have demonstrated the ability to charge and transport micron-sized dust grains in a plasma environment [*Sickafoose et al.*, 2000, 2001, 2002; *Flanagan and Goree*, 2006; *Wang et al.*, 2009]. The Lunar Ejecta and Meteorites experiment (LEAM), deployed by the Apollo 17 astronauts, recorded evidence of slowly moving, highly charged lunar dust moving across the lunar surface near the terminators [*Berg et al.*, 1974]. Additionally, several of the Surveyor spacecraft recorded images of lunar horizon glow just after sunset, which was thought to be forward scattered sunlight due to levitated dust particles [*Criswell*, 1972; *Rennilson and Criswell*, 1974]. Although previous work has addressed both the required conditions and subsequent dynamics of electrostatically charged lunar dust grains [*Nitter and Havnes*, 1992; *Nitter et al.*, 1994, 1998; *Colwell et al.*, 2005; *Borisov and Mall*, 2006; *Stubbs et al.*, 2006; *Farrell et al.*, 2007], these processes are not yet fully understood for the lunar surface. A comprehensive understanding of the plasma environment immediately above the lunar surface will provide a basis for explaining observed lunar dusty plasma phenomena.

[1] Laboratory for Atmospheric and Space Physics, University of Colorado at Boulder, Boulder, Colorado, USA.
[2] Department of Physics, University of Colorado at Boulder, Boulder, Colorado, USA.

0148-0227/10/2010JA015286

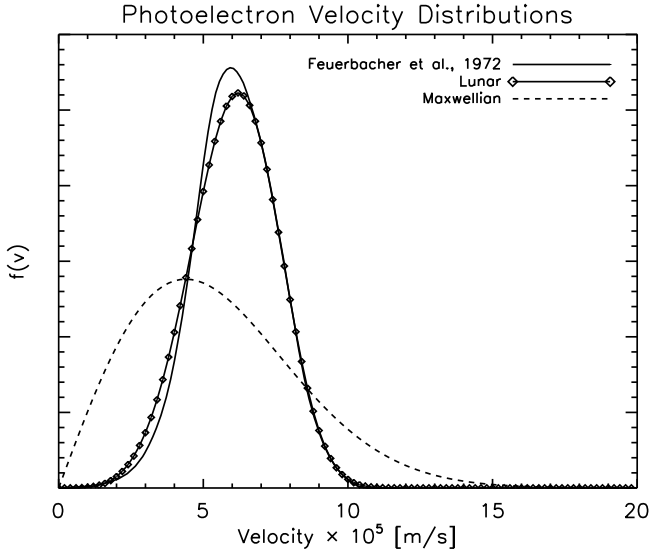

Figure 1. A comparison of the various photoelectron velocity distributions. The solid line is the distribution measured from lunar fines returned by Apollo 17 [*Feuerbacher et al.*, 1972], the diamonds are the function used as the lunar distribution in this paper and the dashed line is the comparable Maxwellian distribution.

[4] In this paper, we present results from a one-dimensional particle-in-cell (PIC) simulation of the photoelectron sheath on the lunar surface. In section 2, we summarize the PIC method and present photoelectron sheath profiles for two different case studies. In section 3, we analyze the ability of these sheaths to charge and levitate dust grains. A discussion and conclusion are presented in section 4.

2. Particle-in-Cell Simulations

[5] In order to simulate the lunar surface plasma environment, a one-dimensional electrostatic particle-in-cell (PIC) code has been developed, following the general outline established by *Birdsall and Langdon* [1985]. The code was validated against analytic solutions for the electron density and electric field profiles, derived for three different photoelectron energy distributions [*Grard and Tunaley*, 1971]. In these cases, the presence of the solar wind was not considered. The theoretical and simulation results show excellent agreement. To customize the code to represent the lunar surface, the left boundary was assigned to be the photoemitting surface and solar wind ions and electrons enter the simulation from the right. All species are absorbed upon reaching the left boundary (lunar surface) and the net surface charge is continuously calculated to maintain charge continuity. While recent observations have shown that a small fraction (~1%) of solar wind protons may be scattered off the lunar surface rather than absorbed [*Saito et al.*, 2008], we do not include such an effect at this time. Photoelectrons that reach the right boundary are re-introduced at the right boundary as solar wind electrons in order to maintain current neutrality at the simulation boundary. All simulations are run long enough in order to ensure that equilibrium conditions are established. In order to resolve the sheath, the ratio of the Debye length, λ_D, to the simulation gridsize was maintained on the order of 25. The total simulation volume was approximately 85–100 λ_D for all simulations. Under nominal solar wind conditions on the lunar dayside, secondary electron emission (via either solar wind electrons or ions) does not represent a significant current [*Willis et al.*, 1973; *Whipple*, 1981] and therefore, has not been included. It is important to note that the lunar surface has a rich variety of topographic relief, as well as a complex magnetic field structure, neither of which are reproducible in a one-dimensional code. Therefore, this model is best representative of a flat plain on the lunar surface at local noon, with either no or an orthogonal magnetic field. Higher dimensionality codes will be able to take into account these, and many other, phenomena.

2.1. Effect of the Photoelectron Energy Distribution and the Solar Wind

[6] The photoelectron energy distribution used in the model is of particular importance as the solar UV-induced photoelectron current is the dominant charging process for the sunlit lunar surface. Previous work has shown that the distribution plays a significant role in determining the photoelectron sheath characteristics [*Grard and Tunaley*, 1971; *Walbridge*, 1973]. The emitted photoelectron energy distribution from lunar fines returned by the Apollo missions has been experimentally measured and arises from the convolution of the solar UV spectrum, the work function, and the photoelectric yield of lunar dust [*Feuerbacher et al.*, 1972]. In our model, we fit the distribution measured by *Feuerbacher et al.* [1972] to a function of the form, $f(v) \propto v^4 e^{-v^4/v_{pe}^4}$, where $v_{pe} = 6.21 \times 10^5$ m/s, shown in Figure 1. This function reproduces several features of the measured distribution, including a strong peak at v_{pe} and a rapid decrease in the amount of higher energy photoelectrons. For our discussions, we shall refer to the measured distribution as the lunar case. To highlight the conditions present on the Moon, a Maxwellian velocity distribution with $kT_{pe} = 2.2$ eV ($v_{th} = 6.21 \times 10^5$ m/s) is also used throughout our analysis as a comparison. The most significant difference between the two distributions is the lack of high-energy (>6 eV) photoelectrons in the lunar distribution. In both cases, the photoelectron emission current density was kept constant at $J_{pe} = 4.5 \times 10^{-6}$ A/m^2 [*Willis et al.*, 1973]. The presence of the incoming solar wind flux was also included in the simulation to accurately represent the lunar surface. Both solar wind ions and electrons are modeled as Maxwellians with $kT_{sw} = 10$ eV with a drift speed of $v_d = 4 \times 10^5$ m/s. Far from the lunar surface ($z > 50\lambda_D$), the plasma is quasi-neutral with a density of $n_e \approx n_i \approx 10^7$ m^{-3}.

[7] Simulation results for the particle densities for both the lunar and Maxwellian sheaths as a function of height are shown in Figure 2. The densities for the individual species (photoelectrons, solar wind electrons and solar wind ions) are shown, as well as the net electron density. The two profiles are qualitatively similar in many respects, including: (1) a high density of photoelectrons for $z \sim <5$ m; (2) a decrease in the solar wind electron density as the solar wind electrons are accelerated towards the positively charged surface; (3) a constant solar wind ion density due to the supersonic velocity of the solar wind ions; and (4) a return to quasineutrality for $z > \sim 25$ m. The major differences between the density profiles is in the photoelectron density, which has a peak

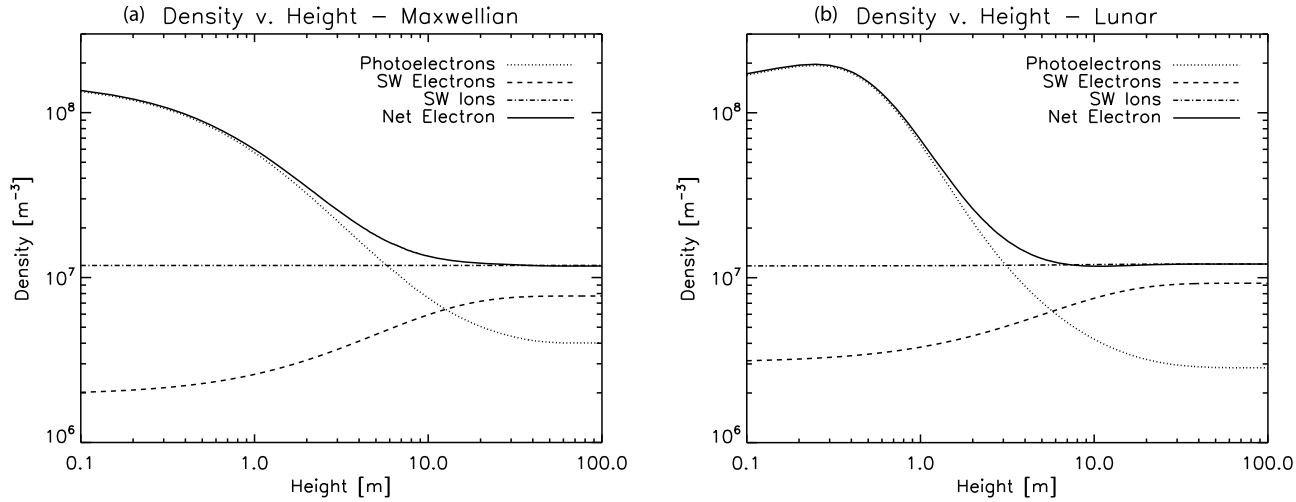

Figure 2. A comparison of the particle densities as a function of height for both the lunar and Maxwellian photoelectron sheaths.

offset from the surface in the lunar case and decreases more rapidly as a function of height. For the Maxwellian case, the model predicts at the surface an electron density of $n_{e,o}$ = 1.5 × 10^8 m^{-3}, Debye length, λ_D = 1.0 m, and electric field E_o = 3.0 V/m, while for the lunar case, the parameters are $n_{e,o}$ = 1.3 × 10^8 m^{-3}, λ_D = 1.1 m and E_o = 3.1 V/m. While the two different cases, Maxwellian and lunar, have similar plasma parameters, their potential profiles differ significantly. As shown in Figure 3a, both cases were found to have non-monotonic potential distributions, as analytically predicted [*Guernsey and Fu*, 1970; *Nitter et al.*, 1998]. Shown in Figure 3b is a comparison of the electric field above the surface for the lunar and Maxwellian cases. The electric field in the lunar photoelectron sheath is weaker than the field in the Maxwellian sheath, mainly due to the lack of high-energy photoelectrons in the lunar distribution. Additionally, due to the non-monotonicity of the potential, both cases have a region of negative, or downward-pointing, electric field. As dust particles are expected to charge positively throughout most of the photoelectron sheath [*Whipple*, 1981; *Horányi*, 1996], regions of negative electric field are unable to support any dust grain levitation. By ~50 m above the surface in both cases, the sheath dies out and the plasma returns to the background, quasi-neutral state of the solar wind.

2.2. Solar UV Variability

[8] A significant source of variability of the lunar surface plasma environment is due to solar UV irradiance. As the sun goes through its eleven year cycle, the UV irradiance can change by several orders of magnitude, with occasional solar flares drastically increasing the solar UV output from solar maximum levels [*Chamberlin et al.*, 2008]. Previous work has shown that conditions at solar maximum and during a solar flare can increase the lunar photoelectric current by factors of three and ten, respectively, from solar minimum conditions [*Sternovsky et al.*, 2008].

[9] We have simulated the lunar photoelectron sheath (as defined in section 2.1) for two additional photoelectron

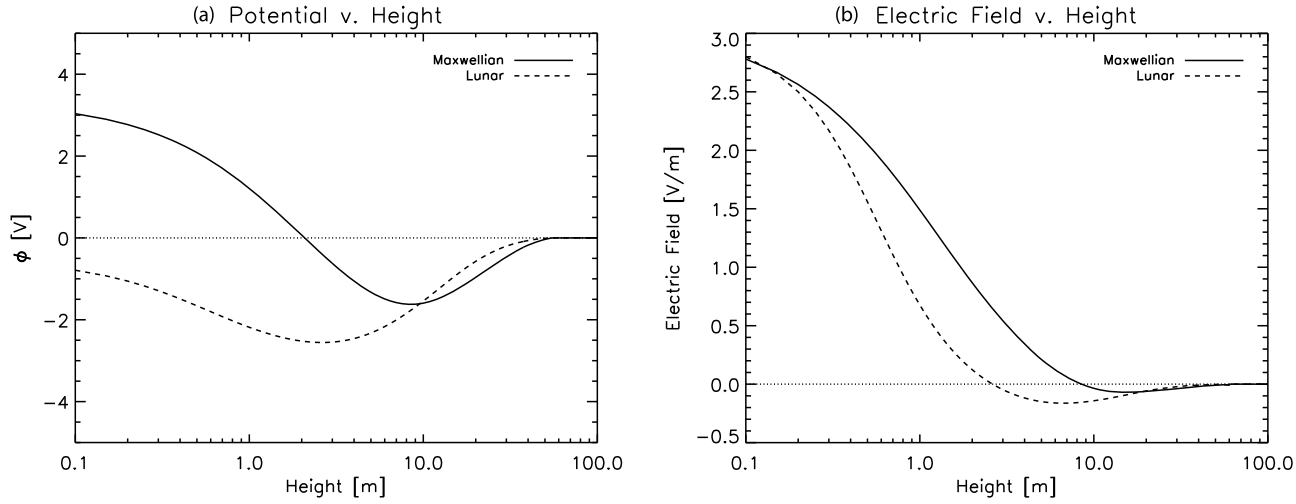

Figure 3. A comparison of the sheath potential and electric field above the surface for both the lunar and Maxwellian photoelectron sheaths.

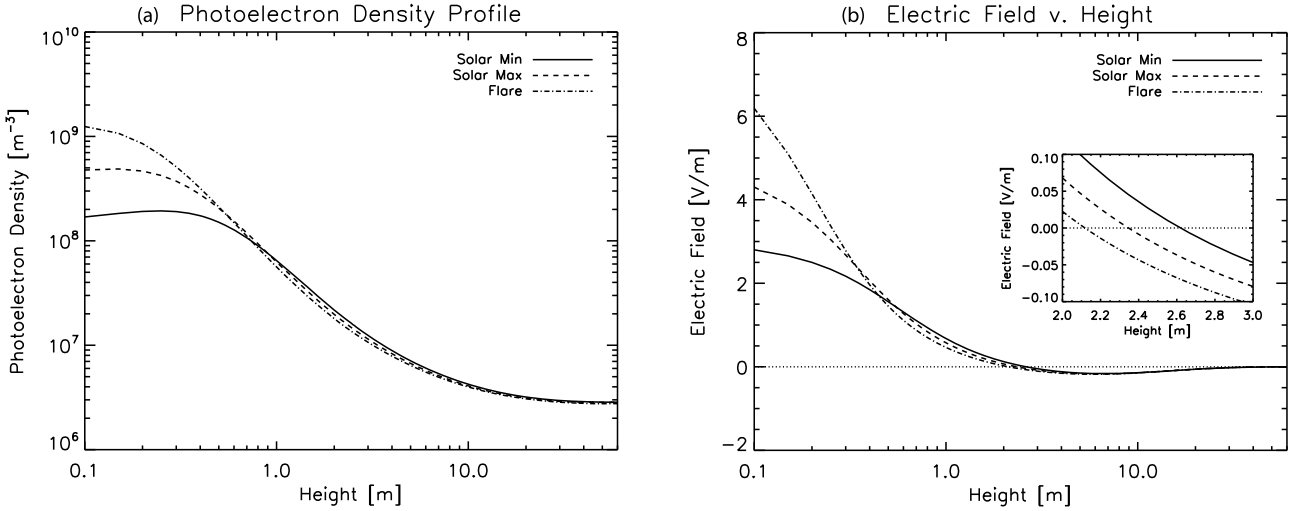

Figure 4. (a) The photoelectron density as a function of height for solar minimum, solar maximum, and flare conditions. An increase in the photoemission current by a factor of ~8 yields a factor of 10 change in the photoelectron density. (b) The electric field as a function of height for all three cases is shown. The surface electric field increases by ~2 from solar minimum to flare conditions. All three conditions still maintain regions of negative electric field. The inset shows an expanded view of the region from 2 to 3 m, where the fields become negative, to highlight the differences among the three cases.

currents, $J_{pe} = 15.5\ \mu\text{A m}^{-2}$ and $45\ \mu\text{A m}^{-2}$, corresponding to solar maximum and flare conditions, respectively. All other parameters have been kept constant. Figure 4 shows the photoelectron density and electric field versus height for the solar minimum, solar maximum and flare conditions. For the photoelectron density, shown in Figure 4a, the increased solar UV irradiance mainly contributes to increasing the density by approximately three and ten for the solar maximum and flare conditions, respectively, from the solar minimum conditions, as was found in previous work [*Sternovsky et al.*, 2008]. For heights greater than 1 m, the density profiles for all three conditions are nearly equivalent, yet small differences are seen due to the nonlinear nature of surface shielding effects. Figure 4b shows an increase of 1.5 and 2 times the solar minimum surface electric field for the solar maximum and flare conditions. These values are significantly lower than those calculated before, which predicted multiplicative increases of 2.5 and 5, respectively [*Sternovsky et al.*, 2008]. These results again show the relative weakness of the electric field in the lunar photoelectron sheath as compared to an equivalent Maxwellian distribution. Shown in the inset in Figure 4b is a subtle, yet important, difference between the three cases. Increased photoemission causes the transition from positive to negative electric field to occur closer to the lunar surface, as the surface charge density is shielded more effectively in the higher current cases.

3. Dust Particle Levitation

[10] The dynamics and equilibria of charged and levitated dust particles above the lunar surface have been previously studied by a number of other models [*Nitter and Havnes*, 1992; *Nitter et al.*, 1994, 1998; *Colwell et al.*, 2005; *Borisov and Mall*, 2006; *Stubbs et al.*, 2006; *Farrell et al.*, 2007]. Here, we model lunar dust charging and dynamics in a time-dependent fashion using the photoelectron sheath profile specific to the lunar surface.

3.1. Levitation Equilibria

[11] A dust particle suspended in a photoelectron sheath will levitate if the electric and gravitational forces on the particle balance. The electric force on the grain is given by $F_e = q_d E$, where q_d is the charge on the grain. This charge is determined from the grain potential, ϕ_d, using the capacitance of a spherical grain, $C_d = 4\pi\epsilon_o a$, where a is the grain radius. The equilibrium grain potential, ϕ_d, which is independent of grain size, is determined as a function of height in the sheath by calculating the grain potential at which the sum of all currents to the grain is zero. The currents included are photoemission, photoelectron collection, and solar wind ion and electron collection [*Whipple*, 1981; *Northrop and Birmingham*, 1996; *Horányi*, 1996]. While recent work has shown that photoemission from micron and sub-micron sized grains may be grain-size dependent [*Abbas et al.*, 2006, 2007], there is some uncertainty regarding the physical mechanism behind this. Therefore, we have not included such an effect at this time. The equilibrium levitation points of the charged dust grain are found by searching for locations where the electric and gravitational forces balance. There are typically two points in the photoelectron sheath at which this condition is satisfied [*Nitter et al.*, 1998; *Robertson et al.*, 2003; *Colwell et al.*, 2005]. By considering the second derivative of the net mechanical potential on the grain, the levitation points can be classified according to their stability. In the cases presented here, the lower point is unstable while the upper point is stable. We perform this analysis for the two case studies presented in section 2: (1) comparison of the Maxwellian and lunar photoelectron distributions, and (2) inclusion of the variability in the solar UV irradiance for the lunar distribution. The plasma densities and electric field are taken from the results of the PIC code for each condition.

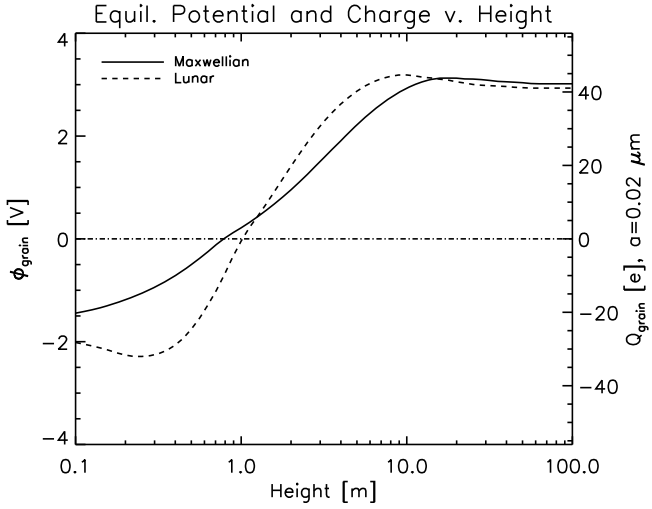

Figure 5. The equilibrium grain potential for both the Maxwellian and lunar cases. Depicted on the right axis is the equilibrium charge for a 0.02 μm grain.

3.1.1. Photoelectron Energy Distribution

[12] Figure 5 shows the grain surface potential, as well as the grain charge for a 0.02 μm grain, as a function of height above the surface for the Maxwellian and lunar cases. Both cases qualitatively show similar curves for the grain potential and charge, however, grains in the lunar case have a lower surface potential and charge closer to the surface and a greater potential and charge farther from the surface than in the Maxwellian case. Above ~10 m, grains in both cases, regardless of size, reach a maximum potential of ~3 V. For a 0.02 μm grain, the potential is equivalent to a grain charge of ~40 e. Figure 6 shows the ratio of the electric to gravitational forces for a 0.02 μm grain for the Maxwellian and lunar sheaths. The Maxwellian case has a consistently higher force ratio than the lunar case due to its stronger electric field. For heights too close to the lunar surface, the force ratio becomes negative due to the negative charge on the grain, while for heights too far from the lunar surface, the ratio becomes negative because of the negative electric field in the sheath. For the particle size presented (a = 0.02 μm), the equilibrium points for the Maxwellian and lunar cases are at ~8.5 m and ~2.5 m, respectively. Thus, for identically sized grains, the lunar sheath cannot support dust levitation as high as the Maxwellian sheath, mainly due to the weaker lunar electric field.

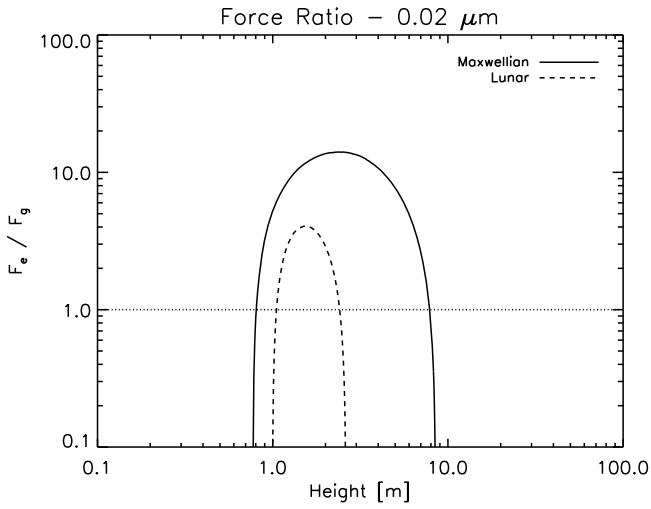

Figure 6. The ratio of the electric to gravitational force for a 0.02 μm grain for both the Maxwellian and lunar cases. The Maxwellian grain has an equilibrium at $z \sim 8.5$ m while the lunar grain has an equilibrium at $z \sim 2.5$ m. The line, $F_e/F_g = 1$ is shown for visual aid.

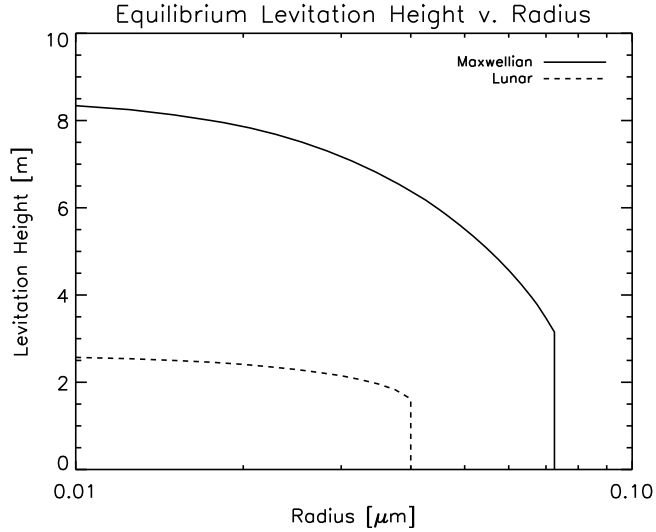

Figure 7. The equilibrium levitation height as a function of particle radius is shown for both the Maxwellian and lunar sheaths. For the Maxwellian case, particles with radii, $r >$ 0.072 μm, cannot be stably levitated in the sheath, while for the lunar sheath, this limit drops to $r >$ 0.04 μm.

[13] Figure 7 shows the stable levitation height for dust grains in the Maxwellian and lunar sheaths as a function of grain radius. An upper limit on the radius of levitating particles as a function of height above the lunar surface can be set at ~0.072 μm and ~0.04 μm for the Maxwellian and lunar cases, respectively. Additionally, particles cannot be levitated higher than ~8.5 m and ~2.5 m, corresponding respectively to the height at which the electric field becomes negative in each case. These values place important constraints on the interpretation of the observations of levitating dust above the lunar surface and are discussed further in section 4.

3.1.2. Solar UV Variability

[14] The increased photoemission for the solar maximum and solar flare conditions increases the sheath electric field and also causes grains to attain a higher charge throughout the sheath. These two effects increase the ability of the sheath to levitate dust grains. Figure 8 shows the equilibrium grain potential and charge for a 0.02 μm grain for the solar minimum, solar maximum and solar flare conditions. The maximum charge on a 0.02 μm grain increases from ~40 e during solar minimum to ~70 e and ~90 e during solar maximum and solar flare conditions, respectively. Additionally, the height at which the grain potential and charge

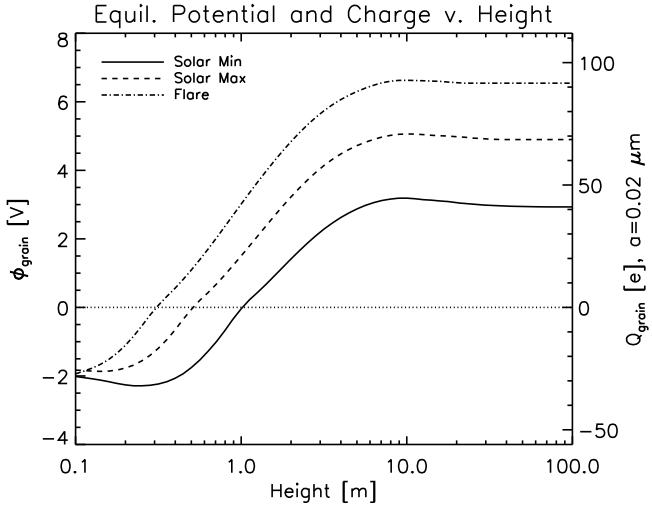

Figure 8. The equilibrium grain potential and charge for a 0.02 μm grain as a function of height above the lunar surface for the solar minimum, solar maximum and solar flare conditions. Increased photoemission leads to a greater equilibrium grain potential and charge.

transition from negative to positive occurs at successively lower heights for increased photoemission.

[15] Using the same analysis as section 3.1.1, the force ratio as a function of height and the equilibrium levitation height as a function of grain radius can be determined for the solar maximum and solar flare conditions. In Figure 9, an increase in the ratio of the electric to gravitational forces on a 0.02 μm grain for both the solar maximum and solar flare conditions is shown. For example, at 1 m, the force ratio for the 0.02 μm grain increases by factors of 10- and 20-fold for the solar maximum and solar flare conditions, respectively.

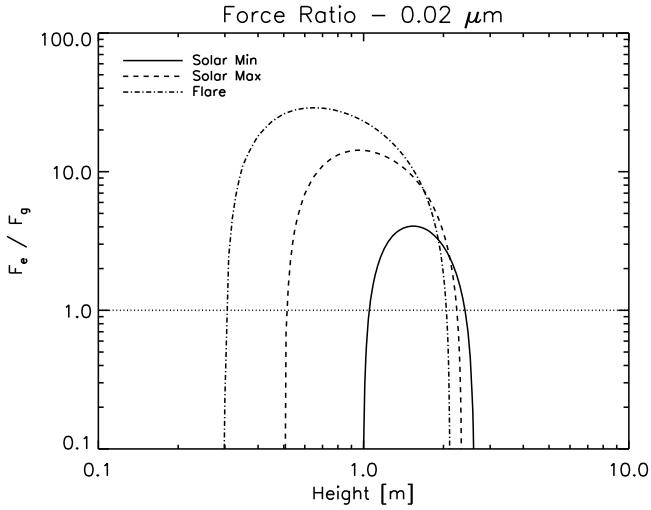

Figure 9. The ratio of the electric and gravitation forces for a 0.02 μm grain is shown as a function of height above the lunar surface for the solar minimum, solar maximum and solar flare conditions. Increased photoemission causes a higher sheath electric field and higher grain charge, leading to an increased ability to levitate dust grains on the lunar surface.

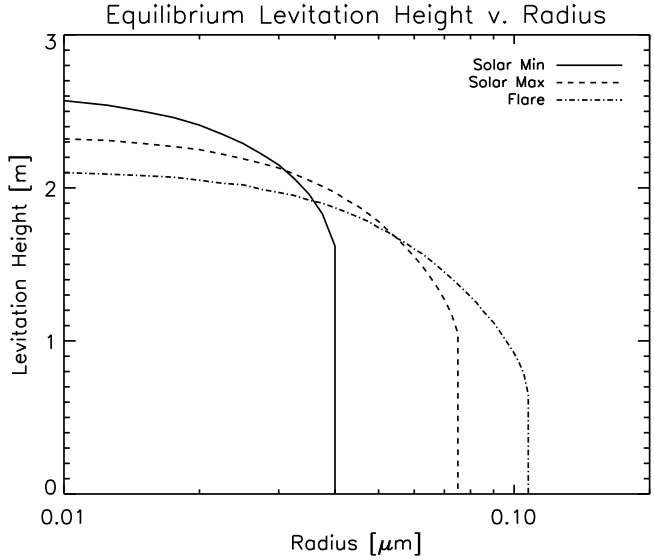

Figure 10. The equilibrium levitation height is shown as a function of particle radius for solar minimum, solar maximum and flare conditions. The increased photoemission current increases the maximum possible levitation grain radius from 0.04 μm at solar minimum to 0.075 μm and 0.12 μm for solar maximum and flare conditions, respectively.

The increase is due to the combination of the increase in the sheath electric field and the increase in the equilibrium grain charge. Figure 10 shows the equilibrium levitation height as a function of grain radius for all three solar UV conditions. The maximum grain radius that can be levitated increases from 0.04 μm for solar minimum conditions, to 0.075 μm and 0.12 μm for solar maximum and flare conditions, respectively. Additionally, the maximum levitation height decreases for increasing solar irradiation, due to the decreasing height of the point at which the sheath electric field becomes negative, as seen in the inset in Figure 4b.

3.2. Levitation Dynamics

[16] Despite the theoretical prediction of stable levitation equilibria for dust grains in both the lunar and Maxwellian sheaths, the accessibility of these equilibria must also be considered. By some mechanism, either micrometeoroid bombardment or electrostatic liftoff, dust grains can be ejected from the surface into the photoelectron sheath. With a set of general initial conditions for grains on the sunlit lunar surface, we can simulate the instantaneous position, velocity and charge of the grain by simultaneously integrating a coupled set of differential equations. The set of differential equations that govern the test particle dynamics and charging are:

$$\frac{dx}{dt} = v \tag{1}$$

$$\frac{dv}{dt} = \frac{qE(x)}{m} - g_{moon} \tag{2}$$

$$\frac{dq}{dt} = I_{ph}(q) - I_{phc}(x,q) - I_{swe}(x,q) + I_{swi}(x,q) \tag{3}$$

where x, v, q and m are the particles' height, velocity, charge, and mass, respectively, g_{moon} is the lunar gravitational acceleration, $E(x)$ is the sheath electric field, and I_{ph}, I_{phc}, I_{swe} and I_{swi} are the photoelectron emission current, photoelectron collection current, solar wind electron current and solar wind ion current, respectively. We explore a broad range of initial velocities for completeness. Typical initial charges for these grains can be estimated by using the surface charge density from the PIC simulations in section 2. For the lunar case, the surface charge density, σ, is approximately 3×10^8 e m^{-2}. With this charge density, only one in one hundred 1.0 μm-sized grains has a single charge. Therefore, in our simulations, we explore grain behavior with either zero or one unit of charge initially. As time evolves, the grain charges discretely with a Monte Carlo type analysis, in order to capture the quantized nature of the grain charge. At each time step, the net current to the grain is calculated, a probability is assigned for the collection or loss an electron, and a random number generator is used to determine if the grain gains or loses a charge. Shown in Figure 11 are the position, velocity and charge for a 0.02 μm grain with initial position, $x_o = 0$, initial velocity, $v_o = 3$ m/s, and initial charge, $q_o = 1$ e during the first 200 s of grain levitation. Within two minutes, the grain oscillates stably between 1 and 4 m, with velocities between ±3 m/s. While not shown, the grain charge reaches an equilibrium of ~20 e within minutes as well. The grain remained stably oscillating for the entire duration of the simulation, more than 15 minutes.

[17] Due to the random charging model of the dust grains, repeated simulations of the same radius and initial velocity will yield different results. Grains that do not attain enough charge during the first pass through the photoelectron sheath will not be able to overcome the gravitational force on the grain. In order to assess the likelihood of stable levitation for dust grains, each combination of radius and initial velocity are traced one hundred times. If the grain levitates for more than ten minutes, it is considered stably levitating. After simulating a large set of grain radii and initial velocities ($0.005 < a < 0.1\mu$m, $0.5 < v_o < 25$ m/s), the region of accessible stable levitation for the lunar sheath was determined to exist for grains less than 0.02 μm and initial velocities less than ~4 m/s. Grains launched with too much initial velocity ($v_o > 4$ m/s), regardless of size, cannot be slowed by the sheath electric field enough to prevent re-impact into the lunar surface. Furthermore, for regions in which stable, dynamically accessible levitation does exist, the probability of stable levitation is less than 20%. The same analysis was repeated for the solar maximum and solar flare conditions. Similar to the solar minimum case, not all theoretical levitation equilibria are dynamically accessible, with limits on the solar maximum case of approximately $a < 0.03$ μm and $v_o < 5$ m/s and on the solar flare case of $a < 0.05$ μm and $v_o < 7$ m/s. In both the solar maximum and solar flare conditions, the probability of levitation increased to ~50% and ~90%, respectively, for the smallest grains.

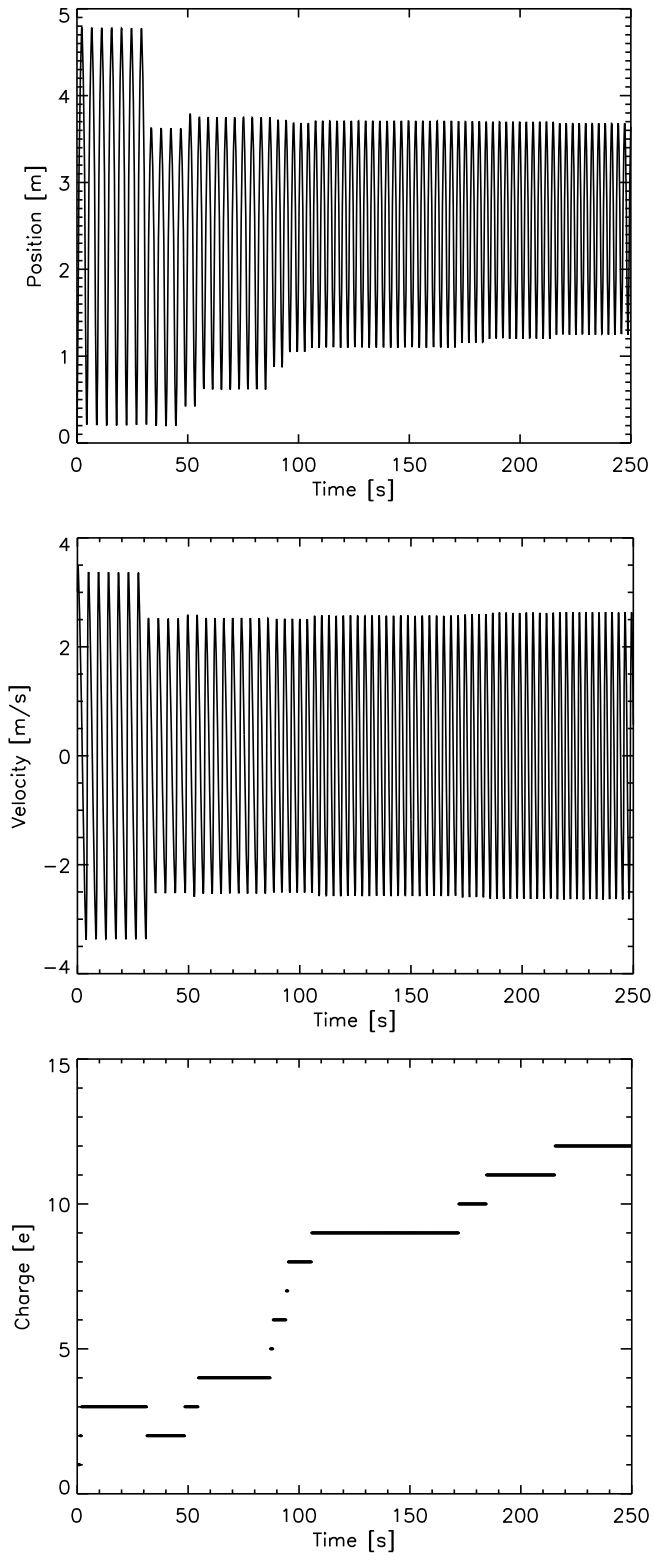

Figure 11. The position, velocity and charge for a 0.02 μm grain, with initial position, $x_o = 0$, initial velocity, $v_o = 3$ m/s and initial charge, $q_o = 1$ e. Discrete jumps in the grain position and velocity are due to the collection or loss of a single electron.

4. Discussion

[18] The lunar photoelectron sheath has been simulated using a PIC method in order to investigate the nature of the lunar plasma environment and to explain observed dusty

plasma phenomena. The model has been applied to four main areas:

[19] 1. Modeling the sunlit, solar-wind exposed lunar surface plasma environment at the sub-solar point: We have found that inclusion of the measured lunar photoelectron velocity distribution predicts a much weaker photoelectron sheath than a sheath with an equivalent Maxwellian distribution. We attribute this to the relative lack of high-energy photoelectrons in the lunar distribution. We have also found that inclusion of the solar wind yields stable non-monotonic potentials in both the lunar and Maxwellian cases, as analytically predicted.

[20] 2. Inclusion of the variability of the solar UV irradiance: By repeating the model with the solar UV irradiance set to solar maximum and solar flare conditions, we predict a change in the photoelectron density of 3 and 10, respectively, and a change in the surface electric field of 1.5 and 2 times, respectively. We suggest that any future measurements or observations of lunar dust activity should be correlated with solar UV irradiation conditions.

[21] 3. Presence of levitation equilibria for sub-micron and micron sized dust grains: Using a test-particle approach, we have calculated the characteristics of levitation equilibria for lunar dust grains at the sub-solar point. The model predicts that both the lunar and Maxwellian sheaths are not capable of supporting electrostatic dust grain levitation for grains with radius, $r > 0.4$ and $r > 0.7$ μm, respectively. A comparison of these limits with previous *in-situ* observations is made below.

[22] 4. Time-dependent charging and dynamics of lunar dust grains: Using the output from the PIC code, combined with a coupled set of differential equations for the grain position, velocity and charge, we have studied the dynamics of lunar dust grains embedded in the photoelectron sheath. The test-particle model predicts that despite the prediction of stable levitation equilibria, not all grain sizes and initial velocities yield stable, electrostatically levitated dust grains above the lunar surface.

[23] Comparison to previous models of the lunar photoelectron sheath and associated dust dynamics highlights some of the important results from this work. *Stubbs et al.* [2006] derived a model concerning the lofting of lunar dust grains, where lofting is defined as the ballistic ejection of micron and sub-micron sized dust grains to altitudes >100 m. While our work has primarily focused on the possibility of electrostatic levitation using both the lunar-specific sheath profiles and time-dependent dust grain charging, our model can be qualitatively compared with the *Stubbs et al.* [2006] model. Notably, the presence of a downward electric field above the photoelectron sheath (due to the non-monotonic potential profile) would decelerate any charged grains (assuming positive charge in sunlight) that were ejected from the surface. While this deceleration would imply a lesser ability to loft grains to km-scale heights, it would not necessarily preclude all grains from being lofted. Additionally, we find no reason why both static levitation and ballistic lofting would not simultaneously be present, albeit with different characteristics. Previous models of electrostatic levitation of dust grains for the asteroid 433 Eros [*Colwell et al.*, 2005] or the Moon [*Nitter and Havnes*, 1992; *Nitter et al.*, 1998; *Colwell et al.*, 2009] differ in their reported maximum levitating grain size. In both models, this is attributable to the assumption of a Maxwellian photoelectron distribution, which, as demonstrated in this model, yields typically stronger electric fields than the lunar photoelectron distribution. Additionally, in the 433 Eros model, the weaker gravity allows levitation of larger particles than an equivalent case on the lunar surface. Notably, the *Nitter et al.* [1998] model included the possibility of non-monotonic potential profiles by including the solar wind influx.

[24] While we assumed that grains on the lunar surface begin with at most a single charge based on the simulated surface charge density, it is theoretically possible that other processes, such as micrometeorite bombardment or energetic particle impact could increase the initial grain charge and therefore increase the likelihood of levitation. Micrometeorite bombardment has been studied before as a possible mechanism for dust grain levitation and lofting [*Rennilson and Criswell*, 1974; *Zook and McCoy*, 1991; *Colwell et al.*, 2005] and has been found insufficient in magnitude to explain various dusty phenomena. Recent laboratory experiments have demonstrated the ability to electrostatically mobilize micron-sized dust grains in a plasma environment similar to the night-side of the Moon [*Wang et al.*, 2009], and such an electrostatic transport mechanism may also be active on the sunlit side of the lunar surface.

[25] Previous analysis of both the Lunar Ejecta and Meteorites experiment (LEAM) measurements of lunar dust transport and the Surveyor images of lunar Horizon Glow have determined the height and size of typical levitated dust grains. *Criswell* [1972] and *Rennilson and Criswell* [1974] have determined a grain radius of $a \sim 6$ μm and levitation height of $h \sim 3$–30 cm for levitated lunar dust grains based on analysis of the Surveyor images. While this grain radius contradicts predictions by the model, the explanation of this discrepancy most likely lies in considering solar illumination effects. Due to the one-dimensional nature of the model presented here, surface topography and oblique solar illumination effects cannot be considered and therefore the model represents a smooth lunar plain at the sub-solar point (solar zenith angle, $\alpha \equiv 0$). While we predict that under such conditions, lunar dust levitation will be extremely unlikely, we cannot make explicit comparison to either the LEAM or the Surveyor measurements. The LEAM experiment was deactivated during most of the lunar day due to instrument overheating [*Berg et al.*, 1974], while for Surveyor, the scattering geometry and the illumination of the lunar surface itself prevented any observations of levitated lunar dust clouds at local noon.

[26] The set of simulations presented here have only begun to explore the richness and complexity of the lunar photoelectron sheath. Many additional factors, including the self-consistent presence of charged, sub-micron and micron-sized dust grains and local lunar topography may have significant effects on the profile of the lunar photoelectron sheath and its ability to charge, mobilize and levitate dust grains. LEAM and Surveyor observations have indicated that the prime region of interest for lunar dust grain levitation is at the terminators, where oblique solar illumination and complex surface topography will significantly alter the near-surface lunar plasma environment. Future work will expand the PIC model

to three-dimensions in order to allow the simulation of the lunar terminators and any associated dust dynamics.

[27] **Acknowledgments.** The authors would like to thank P. Messmer, S. Parker and S. Robertson for several insightful discussions regarding this research. A. Poppe was supported by NASA Headquarters under the NASA Earth and Space Science Graduate Fellowship Program, grant NNX08BA17H. M. Horányi was supported by the Colorado Center for Lunar Dust and Atmospheric Studies of NASA's Lunar Science Institute and by NASA's LASER program, grant NNX08AY77G.

[28] Masaki Fujimoto thanks Masaki Nishino and another reviewer for their assistance in evaluating this paper.

References

Abbas, M. M., et al. (2006), Photoelectric emission measurements on the analogs of individual cosmic dust grains, *Astrophys. J.*, *645*, 324–336.

Abbas, M. M., D. Tankosic, P. D. Craven, J. F. Spann, A. LeClair, and E. A. West (2007), Lunar dust charging by photoelectric emissions, *Planet. Space Sci.*, *55*, 953–965.

Berg, O. E., F. F. Richardson, J. W. Rhee, and S. Auer (1974), Preliminary results of a cosmic dust experiment on the moon, *Geophys. Res. Lett.*, *1*, 289–290, doi:10.1029/GL001i007p00289.

Birdsall, C. K., and A. B. Langdon (1985), *Plasma physics via computer simulation*, McGraw-Hill, New York.

Borisov, N., and U. Mall (2006), Charging and motion of dust grains near the terminator of the moon, *Planet. Space Sci.*, *54*, 572–580.

Chamberlin, P. C., T. N. Woods, and F. G. Eparvier (2008), New flare model using recent measurements of the solar ultraviolet irradiance, *Adv. Space Res.*, *42*, 912–916.

Colwell, J. E., A. A. S. Gulbis, M. Horányi, and S. Robertson (2005), Dust transport in photoelectron layers and the formation of dust ponds on Eros, *Icarus*, *175*, 159–169.

Colwell, J. E., S. Robertson, M. Horányi, X. Wang, A. Poppe, and P. Wheeler (2009), Lunar dust levitation, *J. Aero. Eng.*, *22*, 2–9.

Criswell, D. R. (1972), Lunar dust motion, *Geochim. Cosmochim. Acta., Suppl. 3*, *3*, 2671–2680.

Criswell, D. R., and B. R. De (1977), Intense localized photoelectric charging in the lunar sunset terminator region 2. Supercharging at the progression of sunset, *J. Geophys. Res.*, *82*, 1005–1007.

De, B. R., and D. R. Criswell (1977), Intense localized photoelectric charging in the lunar sunset terminator region 1. Development of potentials and fields, *J. Geophys. Res.*, *82*, 999–1004.

Farrell, W. M., T. J. Stubbs, R. R. Vondrak, G. T. Delory, and J. S. Halekas (2007), Complex electric fields near the lunar terminator: The near-surface wake and accelerated dust, *Geophys. Res. Lett.*, *34*, L14201, doi:10.1029/2007GL029312.

Feuerbacher, B., M. Anderegg, B. Fitton, L. D. Laude, R. F. Willis, and R. J. L. Grard (1972), Photoemission from lunar surface fines and the lunar photoelectron sheath, *Geochim. Cosmochim. Acta., Suppl. 3*, *3*, 2655–2663.

Flanagan, T. M., and J. Goree (2006), Dust release from surfaces exposed to plasma, *Phys. Plasmas*, *13*, 123504, doi:10.1063/1.2401155.

Freeman, J. W., and M. Ibrahim (1975), Lunar electric fields, surface potential and associated plasma sheaths, *Earth Moon Planets*, *14*, 103–114.

Grard, R. J. L., and J. K. E. Tunaley (1971), Photoelectron sheath near a planar probe in interplanetary space, *J. Geophys. Res.*, *76*, 2498–2505.

Guernsey, R. L., and J. H. M. Fu (1970), Potential distribution surrounding a photo-emitting plate in a dilute plasma, *J. Geophys. Res.*, *75*, 3193–3199.

Horányi, M. (1996), Charged dust dynamics in the solar system, *Annu. Rev. Astron. Astrophys.*, *34*, 383–418.

Nitter, T., and O. Havnes (1992), Dynamics of dust in a plasma sheath and injection of dust into the plasma sheath above moon and asteroidal surfaces, *Earth, Moon Planets*, *56*, 7–34.

Nitter, T., T. K. Aslaksen, F. Melandsø, and O. Havnes (1994), Levitation and dynamics of a collection of dust particles in a fully ionized plasma sheath, *IEEE Trans. Plasma Sci.*, *22*, 159–172.

Nitter, T., O. Havnes, and F. Melandsø (1998), Levitation and dynamics of charged dust in the photoelectron sheath above surfaces in space, *J. Geophys. Res.*, *103*, 6605–6620, doi:10.1029/97JA03523.

Northrop, T. G., and T. J. Birmingham (1996), Equilibrium electric potential of spherical, cylindrical, and planar dust grains moving through a plasma, *J. Geophys. Res.*, *101*, 10,793–10,796.

Rennilson, J. J., and D. R. Criswell (1974), Surveyor observations of lunar horizon-glow, *Earth Moon Planets*, *10*, 121–142.

Robertson, S., A. A. S. Gulbis, J. Colwell, and M. Horányi (2003), Dust grain charging and levitation in a weakly collisional plasma sheath, *Phys. Plasma*, *10*, 3874–3880.

Saito, Y., et al. (2008), Solar wind proton reflection at the lunar surface: Low energy ion measurement by MAP-PACE onboard SELENE (KAGUYA), *Geophys. Res. Lett.*, *35*, L24205, doi:10.1029/2008GL036077.

Sickafoose, A. A., J. E. Colwell, M. Horányi, and S. Robertson (2000), Photoelectric charging of dust particles in vacuum, *Phys. Rev. Lett.*, *84*, 6034–6037.

Sickafoose, A. A., J. E. Colwell, M. Horányi, and S. Robertson (2001), Experimental investigations of photoelectric and triboelectric charging of dust, *J. Geophys. Res.*, *106*, 8343–8356, doi:10.1029/2000JA000364.

Sickafoose, A. A., J. E. Colwell, M. Horányi, and S. Robertson (2002), Experimental levitation of dust grains in a plasma sheath, *J. Geophys. Res.*, *107*(A11), 1408, doi:10.1029/2002JA009347.

Sternovsky, Z., P. Chamberlin, M. Horányi, S. Robertson, and X. Wang (2008), Variability of the lunar photoelectron sheath and dust mobility due to solar activity, *J. Geophys. Res.*, *113*, A10104, doi:10.1029/2008JA013487.

Stubbs, T. J., R. R. Vondrak, and W. M. Farrell (2006), A dynamic fountain model for lunar dust, *Adv. Space Res.*, *37*, 59–66.

Walbridge, E. (1973), Lunar photoelectron layer, *J. Geophys. Res.*, *78*, 3668–3687.

Wang, X., M. Horányi, and S. Robertson (2009), Experiments on dust transport in plasma to investigate the origin of the lunar horizon glow, *J. Geophys. Res.*, *114*, A05103, doi:10.1029/2008JA013983.

Whipple, E. C. (1981), Potentials of surfaces in space, *Rep. Prog. Phys.*, *44*, 1197, doi:10.1088/0034-4885/44/11/002.

Willis, R. F., M. Anderegg, B. Feuerbacher, and B. Fitton (1973), Photoemission and secondary electron emission from lunar surface material, in *Photon and Particle Interactions With Surfaces in Space*, edited by R. J. L. Grard, pp. 369–387, Springer, New York.

Zook, H. A., and J. E. McCoy (1991), Large scale lunar horizon glow and a high altitude lunar dust exosphere, *Geophys. Res. Lett.*, *18*, 2117–2120, doi:10.1029/91GL02235.

M. Horányi and A. Poppe, Department of Physics, University of Colorado at Boulder, UCB 392, Boulder, CO 80309, USA. (horanyi@colorado.edu; poppe@lasp.colorado.edu)